



OPEN

Phase-locking and Pulse Generation in Multi-Frequency Brillouin Oscillator via Four Wave Mixing

SUBJECT AREAS:
NONLINEAR OPTICS
OPTICS AND PHOTONICSThomas F. S. Büttner¹, Irina V. Kabakova¹, Darren D. Hudson¹, Ravi Pant¹, Christopher G. Poulton^{1,2}, Alexander C. Judge¹ & Benjamin J. Eggleton¹Received
6 February 2014Accepted
2 May 2014Published
22 May 2014Correspondence and
requests for materials
should be addressed to
T.F.S.B. (thomasb@
physics.usyd.edu.au)
or B.J.E. (egg@physics.
usyd.edu.au)¹Centre for Ultrahigh bandwidth Devices for Optical Systems (CUDOS), Institute of Photonics and Optical Science (IPOS), School of Physics, University of Sydney, NSW, 2006, Australia, ²CUDOS, School of Mathematical Sciences, University of Technology, Sydney, NSW, 2007, Australia.

There is an increasing demand for pulsed all-fibre lasers with gigahertz repetition rates for applications in telecommunications and metrology. The repetition rate of conventional passively mode-locked fibre lasers is fundamentally linked to the laser cavity length and is therefore typically $\sim 10\text{--}100$ MHz, which is orders of magnitude lower than required. Cascading stimulated Brillouin scattering (SBS) in nonlinear resonators, however, enables the formation of Brillouin frequency combs (BFCs) with GHz line spacing, which is determined by the acoustic properties of the medium and is independent of the resonator length. Phase-locking of such combs therefore holds a promise to achieve gigahertz repetition rate lasers. The interplay of SBS and Kerr-nonlinear four-wave mixing (FWM) in nonlinear resonators has been previously investigated, yet the phase relationship of the waves has not been considered. Here, we present for the first time experimental and numerical results that demonstrate phase-locking of BFCs generated in a nonlinear waveguide cavity. Using real-time measurements we demonstrate stable 40 ps pulse trains with 8 GHz repetition rate based on a chalcogenide fibre cavity, without the aid of any additional phase-locking element. Detailed numerical modelling, which is in agreement with the experimental results, highlight the essential role of FWM in phase-locking of the BFC.

Stimulated Brillouin Scattering (SBS), whereby light interacts coherently with acoustic phonons, is one of the strongest nonlinear effects observed in optical fibres^{1–3}. In the SBS process, a narrow-band pump field of frequency ω_0 can generate a strong backward-propagating Stokes field of frequency $\omega_1 = \omega_0 - \Omega_B$ through interaction with acoustic phonons (frequency Ω_B) once a certain power threshold is reached. Although SBS in optical fibres can be detrimental to optical systems, it has also enabled a range of important technologies such as Brillouin fibre lasers^{4–6}, amplifiers², sensors⁷, pulse compressors⁸, phase conjugators⁹, as well as devices for slow light^{10–12}, stored light¹³, laser cooling of vibrational modes¹⁴, low phase-noise microwave oscillators¹⁵, and all-optical signal processing^{16,17}.

Brillouin lasing is achieved by generating Stokes photons via SBS in a cavity^{4–6}. Due to the cavity feedback, the power threshold for the generation of the Stokes waves is reduced considerably¹⁸. The linewidth of the Stokes field can then be much narrower than the Brillouin gain bandwidth $\Delta\nu_B = 1/(2\pi\tau)$, where τ is the phonon lifetime³. In Brillouin lasers with short cavities, i.e. cavities short enough such that the free spectral range (FSR) of the cavity is of the order of the gain bandwidth $\Delta\nu_B$, only one cavity mode experiences strong Brillouin gain. Such lasers emit a single frequency Stokes wave once the lasing threshold is reached. In the general (off-resonant) case, the peak of the SBS gain spectrum ($\omega_0 - \Omega_B$) does not coincide with a cavity resonance and the frequency of the Stokes wave ω_1 is determined by an interplay between Brillouin gain, nonlinear phase-shift from the Kerr-nonlinearity, and cavity selectivity, known as Stokes detuning¹⁹.

SBS can be cascaded in resonators, which produces multiple, frequency shifted Stokes waves, thus forming a Brillouin frequency comb²⁰. The spectral lines of BFCs are spaced by the Brillouin frequency shift Ω_B which is determined by the acoustic properties of the medium ($\Omega_B/2\pi \approx 10$ GHz for glasses) and is independent of the resonator length. BFCs have been demonstrated in different configuration, such as Fabry-Perot cavities^{18,20}, phase-conjugate resonators²¹, fibre ring cavities²², Brillouin-erbium fibre lasers²³ and micro-resonators^{6,15,24}. Phase-locking of such combs holds a promise to achieve pulsed laser sources with gigahertz repetition rates^{25,26}. This is orders of magnitude larger than the repetition rates of conventional passively mode-locked fibre lasers



which are fundamentally linked to the laser cavity length and therefore are typically of the order of 10–100 megahertz²⁷.

In the absence of any additional nonlinear effect than SBS, phase-locking of BFCs can only be achieved by coupling all Stokes waves with a common acoustic wave. Yet, in resonators with a single optical transverse mode, acoustic waves that couple adjacent comb components have different propagation constants^{19,28}. Coupling multiple Stokes waves with a single acoustic wave is thus problematic: the interaction is not phase-matched and becomes inefficient over distances greater than a few millimeters²⁵. In resonators that allow SBS interaction over longer lengths, each Stokes wave is formed through stimulated scattering from a new acoustic wave. In this process, the Stokes waves attain random phases as each acoustic wave grows from noise²⁹. In addition, phase-noise and unequally spaced comb components, due to different detunings of the Stokes waves, lead to a changing spectral phase of the BFC with time.

Different cavity configurations have been suggested to achieve phase-locking of BFCs^{21,25,26,30}. Experimentally, phase-locking of BFCs has been demonstrated by achieving coupling of all Stokes waves with a common acoustic wave by limiting the SBS interaction to a short part of the cavity²¹ and by using modal dispersion in a short-multimode fibre³⁰. Recently, an autocorrelation measurement of a Brillouin comb generated in a Brillouin-erbium fibre laser has been presented that suggests pulse-like behaviour in the time domain³¹. However, the phase-locking mechanism for this configuration has not been explained and the autocorrelation presented is not unambiguous evidence of a pulse train due to a relatively large autocorrelation background³².

Kerr-induced four wave-mixing (FWM) also leads to generation of new frequencies and, unlike SBS, is known to couple three or more optical waves in a phase-sensitive manner^{3,33}. It has been shown that frequency combs generated through cascaded FWM in high-finesse micro-resonators can exhibit certain spectral phase signatures³⁴. Recently, phase-locking and generation of temporal solitons have also been observed in such a configuration³⁵.

In resonators, SBS and FWM can efficiently co-exist. Degenerate FWM between co-propagating pump and Stokes waves (generated via SBS) create Anti-Stokes waves at frequencies $\omega_j = \omega_0 - j \times \Omega_B$, for $j < 0$, and higher-order Stokes waves at frequencies $\omega_j = \omega_0 - j \times \Omega_B$ for $j \geq 2$. Generation of Anti-Stokes waves is a clear sign of the presence of FWM since these waves cannot be generated by SBS. The Stokes waves generated via FWM, in turn, can act as a seed and can be further amplified by SBS, thus reducing the threshold for higher-order Stokes waves^{36–39}. Steady state powers of Stokes and anti-Stokes waves formed by the interplay of SBS and FWM in a Fabry-Perot cavity have previously been studied theoretically⁴⁰, however in this earlier study the authors were only interested in the time-averaged steady state powers and the phase-relationship between the waves was not considered.

In this work, we demonstrate for the first time numerical and experimental results that show the generation of phase-locked BFCs with repeatable spectral phase via the interplay of SBS and FWM. Real-time measurements of the comb show stable picosecond pulse trains with GHz repetition rate. Our experiment was performed in a short (~38 cm), low finesse, Fabry-Perot fibre cavity. A detailed numerical study of the system shows good agreement with experimental results and clearly establishes that FWM is essential for the system's dynamics to attain a phase-locked steady state.

This new understanding of the interaction between FWM and SBS can potentially be exploited for creating novel picosecond pulse sources with GHz repetition rate for optical communication systems, metrology and high speed optical clocks⁴¹.

Results

BFCs were generated by coupling quasi-continuous wave (quasi-CW) pump light into a Fabry-Perot cavity consisting of a short piece

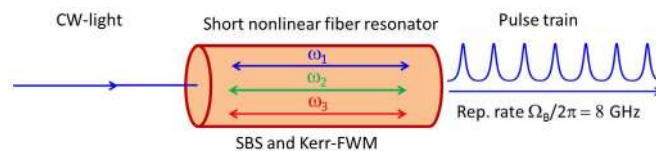


Figure 1 | Concept of pulse train generation via SBS and FWM. CW light is coupled into a short, nonlinear fibre resonator. New frequencies are generated via SBS and FWM. At the output a train of phase-locked pulses can be observed with repetition rate equal to the SBS frequency shift.

of As_2Se_3 chalcogenide glass⁴² fibre as illustrated schematically in Fig. 1. Quasi-CW light was used to avoid thermal effects by keeping the average power low (~10 mW) while obtaining high peak powers (~1 W). The pump light consisted of narrow band 500 ns square pulses at 1550 nm. The polarisation of the pump was adjusted such that only one polarisation mode was excited. Due to a large refractive index of $n = 2.81$, the Fresnel reflections on the perpendicularly cleaved fibre facets provided feedback of about $R = 22.6\%$. A single transverse mode with an effective area of $A_{\text{eff}} = 56 \mu\text{m}^2$ was guided by the fibre. The large Brillouin gain^{43,44} $g_B = 6.10 \times 10^{-9}$ m/W and nonlinear refractive index⁴⁵ $n_2 = 2.4 \times 10^{-13}$ cm²/W of the chalcogenide glass allowed us to perform the experiment in a short fibre length $L = 38.29$ cm. The phonon lifetime⁴³ in As_2Se_3 is $\tau = 1/(2\pi\Delta\nu) = 12$ ns. The Brillouin frequency shift and the FSR of the fibre cavity were measured to be $\Omega_B/(2\pi) = 7.805$ GHz and $\text{FSR} = 139.3$ MHz, respectively. The fibre length L was chosen such that it was long enough to allow generation of cascaded Stokes waves via SBS at peak intensities well below the damage threshold of As_2Se_3 and to be short enough that only one cavity mode experiences strong Brillouin gain ($\text{FSR} > \Delta\nu$). The linear propagation loss of the As_2Se_3 fibre⁴³ is $\alpha = 0.84$ dB/m and the dispersion coefficient⁴² is about $D = -504$ ps km⁻¹nm⁻¹. Details about the experimental setup can be found in the Methods section.

Important parameters of the system dynamics⁴⁰ are the linear phase-shift $\Delta\varphi_j$ of the pump ($j = 0$) and Stokes waves ($j = 1, 2, \dots$) per cavity roundtrip. It is convenient to describe these linear phase shifts in the form

$$\Delta\varphi_j = \Delta\varphi_0 - j\beta, \quad (1)$$

where $\Delta\varphi_0 = 2\omega_0 nL/c$ is the linear phase shift of the pump per round trip and $\beta = 2\Omega_B nL/c$ is the difference of the linear phase shifts of the two adjacent comb components per round trip (without Stokes detuning). Here, we neglected the dispersion of the effective index n and the Brillouin shift Ω_B because we only consider a small frequency range (~30 GHz). Since $\Delta\varphi_0$ represents an absolute phase, it is sensitive to small changes of n and L due to temperature drift of the cavity and also to tuning the frequency ω_0 of the pump laser. In the experiment $\Delta\varphi_0$ has not been stabilised and its values are unknown. The parameter β is a phase-difference and is far less sensitive to pump tuning and temperature drift than $\Delta\varphi_0$ and is assumed to be constant in the parameter range considered here. For both experiments and simulations, β was a multiple of 2π . However, we found that this is not the only condition for observing phase-locking and qualitatively similar results were also obtained in experiments and simulations for different values of β .

Experiment. Figure 2(a) shows the optical spectrum of the input light. The spectrum consists of a single line at $\lambda = 1550.2$ nm corresponding to the pump light (P). A time domain measurement of the input light is plotted in the inset in Fig. 2(a), showing a square pulse of 500 ns length with a slight slope decreasing toward the end of the pulse arising from the amplification process. A typical spectrum measured at the output of the chalcogenide fibre for about 0.7 W peak power coupled into the fibre is plotted in Fig. 2(b). Besides the pump light (P) the output spectrum also

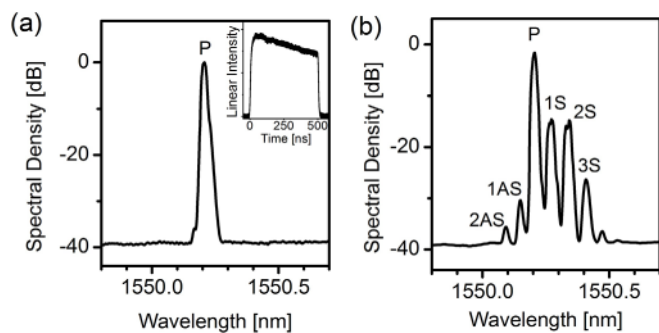


Figure 2 | Optical spectra of input and output light of the fibre resonator. (a) Spectrum of the input light consisting of a single pump frequency (P). The inset shows the temporal measurement of a 500 ns input pulse. (b) Averaged output spectrum of the fibre resonator for about 0.7 W input peak power. Besides the pump (P), Stokes waves (1S–3S) at longer wavelength as well as anti-Stokes waves (1AS, 2AS) at shorter wavelengths are visible.

exhibits three Stokes lines at longer wavelength (1S–3S) and two anti-Stokes waves (1AS, 2AS) at shorter wavelengths compared to the pump (P). The Stokes waves (1S–3S) were generated through the interplay of SBS and FWM and the anti-Stokes waves (1AS, 2AS) were generated through FWM of pump and Stokes waves^{18,46}. The spacing between two neighboring lines is about $\Delta\lambda = 63$ pm, which is equal to the SBS frequency shift of the As_2Se fibre $\Delta\lambda = \Omega_B\lambda^2/(2\pi c)$ at $\lambda = 1550$ nm.

Two real-time measurements of output light from the chalcogenide fibre cavity are shown in Fig. 3(a) and 3(b) for the input powers of about 0.7 W but for different values of $\Delta\phi_0$. Recall that the phase shift $\Delta\phi_0$ could be changed by tuning the frequency ω_0 of the pump laser. The insets to (a) and (b) show zoomed-in sections of 1 ns time intervals of the main graph. Compared to the input quasi-CW pulses, the output pulses show rapid temporal interference signals after about 25 ns which are not resolved in the main graph. The inset at about 30 ns in Fig. 3(a) reveals a cosine oscillation, which we attribute to beating between the pump and the newly generated first Stokes wave^{3,28}. The frequency of the beat signal corresponds to $\Omega_B/(2\pi)$, *i.e.* the Brillouin frequency shift.

We first consider envelopes of the interference signals in Fig. 3(a) and 3(b). In Fig. 3(a) the envelope of the interference signal is modulated with a period of approximately 100 ns, whereas a constant envelope of the interference signal can be seen in Fig. 3(b). The two insets (at 246 ns and 373 ns) in Fig. 3(a) reveal a strong second frequency of $2 \times \Omega_B/(2\pi)$. The spectrum shown in Fig. 2(b) suggests that the main contribution to this higher frequency is a result of interference between the pump and second-order Stokes wave. It is clear from the insets that the interference signal of the multiple waves in Fig. 3(a) is not constant throughout the 500 ns pump duration and that the phase-relationship of the waves drifts in time (at the rate of approximately $1/100$ ns = 10 MHz). This drift arises from non-equally-spaced comb lines resulting from different Stokes detunings of the first and second-order Stokes waves.

Figure 3(b) shows a qualitatively different result obtained for a different value of $\Delta\phi_0$. After about 100 ns the system reaches a steady state with a constant envelope of the modulation. The zoomed-in sections of the interference signal, shown in the insets at 200 ns and 400 ns reveal a stable train of ~ 40 ps sub-pulses with a repetition rate of $\sim \Omega_B/(2\pi)$. The pulse shape is the result of the interference of at least 3 waves (such as pump, first and second-order Stokes wave) equally spaced in frequency and with a constant phase relationship.

This phase-locked train of pulses is repeatable and stable if the experiment is repeated with the same experimental conditions. We

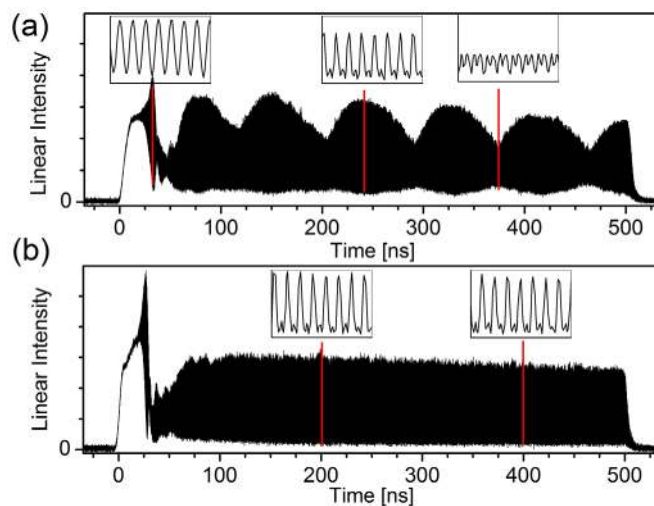


Figure 3 | Temporal measurements of output pulses. (a), (b) Output pulses of the fibre resonator for 500 ns input pulses for two different values of the phase-shift $\Delta\phi_0$. The insets show zoomed in sections of 1 ns length at different times. Both measurements were taken for similar input powers of ~ 0.7 W.

demonstrated this by recording the output pulses for a series of input pump pulses. Figure 4(a) shows 11 output pulses observed for 11 independent 500 ns input pulses coupled into the fibre with 0.5 ms delay between the pulses. All output pulses display very similar temporal behavior. Figure 4(b) shows a 0.5 ns long zoomed-in section of the output pulses at 325 ns, revealing the same interference of the waves for all traces. From this we conclude that the waves that contribute the interference have the same phase-relationship for all measurements.

Numerical study. The experiment indicates that a stable train of pulses can be obtained with a phase-relationship of the contributing waves, which is repeatable and constant in time. As outlined above, SBS alone does not possess a mechanism to provide either of these properties.

We believe that FWM can explain phase-locking with a repeatable phase-relationship. We demonstrated this by performing a numerical study of the system with and without FWM and compared the simulation results. For the sake of simplicity we only present results for the smallest number of waves that are necessary to qualitatively reproduce the experimental results in this paper and to demonstrate the phase-locking mechanism.

The model includes forward and backward propagating pump, first and second-order Stokes waves, and the corresponding four acoustic waves which couple these waves in a fibre oriented along the z -direction. The interaction between these six optical and four acoustic waves can be described in terms of the dynamic coupled mode-equations¹⁹ (S3)–(S7) shown in the Supplementary Information. In these equations we included terms relevant to the SBS interaction, as well as the effects arising from the Kerr-nonlinearity: self-phase modulation (SPM), cross-phase modulation (XPM) and FWM. Simulation parameters were chosen to match experimental conditions. The boundary conditions used in the simulation are given in equations (S8) in the Supplementary Information. Reflections from the facets of the fibre cavity and the linear phase-shifts of pump and Stokes waves per cavity roundtrip described by $\Delta\phi_j$ (see equation (1)) have been considered. Information on how the coupled mode-equations were integrated can be found in the Methods section.

To compare simulation and experimental results we look at the optical power at the output of the fibre. The optical (pump ($j = 0$),

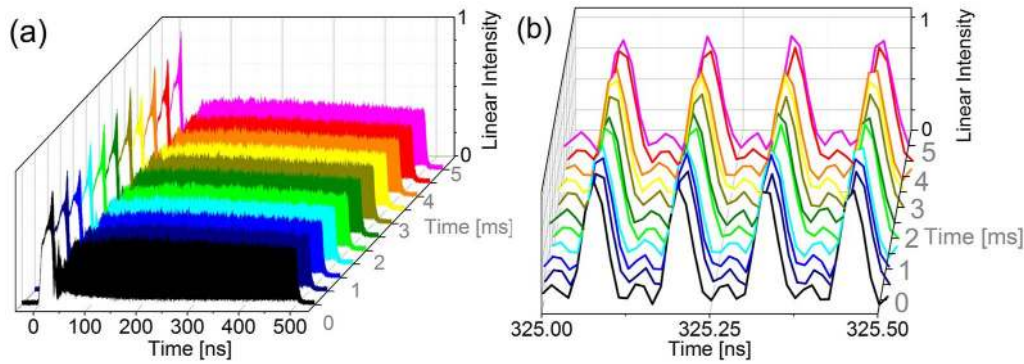


Figure 4 | Temporal stability. Temporal measurements of a series of eleven independent output pulses recorded in a 5 ms time interval with 0.5 ms time separation between the measurements. (a) Showing the entire 500 ns output pulses. (b) 0.5 ns long zoomed-in section of the pulses shown in (a) at 325 ns. (The maxima are aligned for better visibility.)

first ($j = 1$) and second ($j = 2$) Stokes) waves in the fibre resonator can be described in terms of the complex amplitudes $E_j^\pm(z, t)$ of their electric fields:

$$E_j^\pm(z, t) = A_j^\pm(z, t) e^{-i\omega_j(t \mp nz/c)} = \sqrt{P_j^\pm(z, t)} e^{i\theta_j^\pm(z, t)}; \quad j=0,1,2. \quad (2)$$

Here “ \pm ” indicates the direction of propagation, $A_j^\pm(z, t)$ are the slowly varying complex envelopes of the amplitudes $E_j^\pm(z, t)$. $\theta_j^\pm(z, t) = \varphi_j^\pm(z, t) - \omega_j(t \mp nz/c)$ represent the phases of the waves, $n \approx 2.81$ is the effective index, and ω_j are the steady state frequencies of the waves. We assume that the complex amplitudes $E_j^\pm(z, t)$ are normalized such that $P_j^\pm(z, t)$ represent the optical powers of the waves measured in dimensions of Watts. The output power $P_{\text{out}}(t)$ at the end of the fibre resonator can be calculated with

$$P_{\text{out}}(t) = (1 - R) |E_0^+(L, t) + E_1^+(L, t) + E_2^+(L, t)|^2. \quad (3)$$

In order to obtain stable pulses at the output of the fibre, the powers $P_j^\pm(z, t)$ and the phases $\varphi_j^\pm(z, t)$ must attain a steady state. The total output power $P_{\text{out}}(t)$ in the steady state can be calculated by inserting equation (2) into equation (3) to yield

$$\begin{aligned} P_{\text{out}}(t)/(1 - R) &= P_0^+(L) + P_1^+(L) + P_2^+(L) \\ &+ 2\sqrt{P_0^+(L)P_1^+(L)} \cos[(\omega_0 - \omega_1)(t - t_0)] \\ &+ 2\sqrt{P_1^+(L)P_2^+(L)} \cos[\vartheta^+(L, t) + (\omega_0 - \omega_1)(t - t_0)] \\ &+ 2\sqrt{P_0^+(L)P_2^+(L)} \cos[\vartheta^+(L, t) + 2(\omega_0 - \omega_1)(t - t_0)], \end{aligned} \quad (4)$$

where $t_0 = [\varphi_0^+(L) - \varphi_1^+(L)]/(\omega_0 - \omega_1) + nL/c$ is a constant time offset. In Equation (4) we have introduced the phase parameter

$$\begin{aligned} \vartheta^\pm(z, t) &= \theta_0^\pm(z, t) - 2\theta_1^\pm(z, t) + \theta_2^\pm(z, t) \\ &= \varphi_0^\pm(z, t) - 2\varphi_1^\pm(z, t) + \varphi_2^\pm(z, t) \\ &- \left(t \mp \frac{nz}{c} \right) [(\omega_0 - \omega_1) - (\omega_1 - \omega_2)]. \end{aligned} \quad (5)$$

$\vartheta^\pm(z, t)$ express the phase relationships between the three forward and backward propagating electric fields $E_1^+(z, t)$, $E_2^+(z, t)$, $E_3^+(z, t)$ and $E_1^-(z, t)$, $E_2^-(z, t)$, $E_3^-(z, t)$, respectively. The values of $\vartheta^\pm(z, t)$ are critical for the phase-sensitive FWM interaction between the waves³³. Depending on the phase-relationships $\vartheta^\pm(z, t)$, power flows from the first Stokes to the pump and the second Stokes or the other way around. Furthermore, the sign and the magnitude of nonlinear phase-shifts caused by FWM depend on $\vartheta^\pm(z, t)$ (see Supplementary Information equations (S10–S15)). Equation (5) shows that even

when the powers $P_j^+(L, t)$ and the phases $\varphi_j^+(L, t)$ are independent of time, $\vartheta^+(L, t)$ drifts with a constant rate if the frequencies ω_j are not equally spaced, preventing a stable interference signal $P_{\text{out}}(t)$. The steady state frequencies ω_1 and ω_2 of the Stokes waves are determined by a complicated interplay of Brillouin gain, nonlinear phase-shift from the Kerr-nonlinearity and cavity selectivity. In general, different order Stokes waves experience different amounts of Stokes detuning and the frequencies of the three waves are not equally spaced. Additionally, in order to obtain short pulses (of length $\sim 2\pi/(N\Omega_B)$, where N is the number of participating waves²⁶), $\vartheta^+(L, t)$ must also be close to zero to achieve the appropriate phasing of the three waves.

To illustrate the effect of FWM we first performed the simulations with and without FWM interaction while the terms for SBS, SPM and XPM remained in the equations.

Figure 5(a) and 5(b) show two qualitatively different results that were obtained by including FWM in the simulation, consistent with experimental conditions. Both simulations were performed using the estimated coupled input power of the experiment $P_{\text{in}} = 0.7$ W. For the parameter $\Delta\varphi_0$ we choose $\Delta\varphi_0 = 0.548\pi$ and $\Delta\varphi_0 = 1.2\pi$, respectively, in order to obtain results that are qualitatively similar to the experimental results shown in Fig. 3(a) and 3(b). The plots on the left show the evolution of the powers $P_j^+(L, t)$ and the phase parameter $\vartheta^+(L, t)$ whereas the plots on the right display the output power of the fibre $P_{\text{out}}(t)$. The insets of the plots on the right show 1 ns long zoomed-in sections at different times. In Fig. 5(a) ($\Delta\varphi_0 = 1.2\pi$) neither the powers $P_j^+(L, t)$ nor the parameter $\vartheta^+(L, t)$ reach a steady state so the envelope of the burst is modulated and the pulses are not stable. However, for $\Delta\varphi_0 = 0.548\pi$ in Fig. 5(b) the phase parameter $\vartheta^+(L, t)$ and the powers $P_j^+(L, t)$ reach a steady state after an initial power transfer from pump to the Stokes waves. Since the powers $P_j^+(L, t)$ and $\vartheta^+(L, t)$ are independent of time, a stable train of pulses can be obtained.

Figure 5(c) shows simulation results obtained when FWM was not included in the simulation. The same parameters were used that generated the results of Fig. 5(b) ($P_{\text{in}} = 0.7$ W, $\Delta\varphi_0 = 0.548\pi$). After an initial power transfer to the Stokes waves, the powers $P_j^+(L, t)$ of all waves reach a steady state^{3,28}. However, $\vartheta^+(L, t)$ drifts at a constant rate, which is the result of unequally spaced frequencies. Since $\vartheta^+(L, t)$ is not constant the interference signal changes with time and has a modulated envelope (Fig. 5(c), right).

The results of the simulation demonstrate that FWM links the parameter $\vartheta^\pm(z, t)$ to the powers $P_j^\pm(z, t)$ and *vice versa*. This important contribution of FWM is also illustrated by the steady state equations (S10)–(S15) shown in the Supplementary Information. The FWM terms (and only these terms) contain the phase parameters

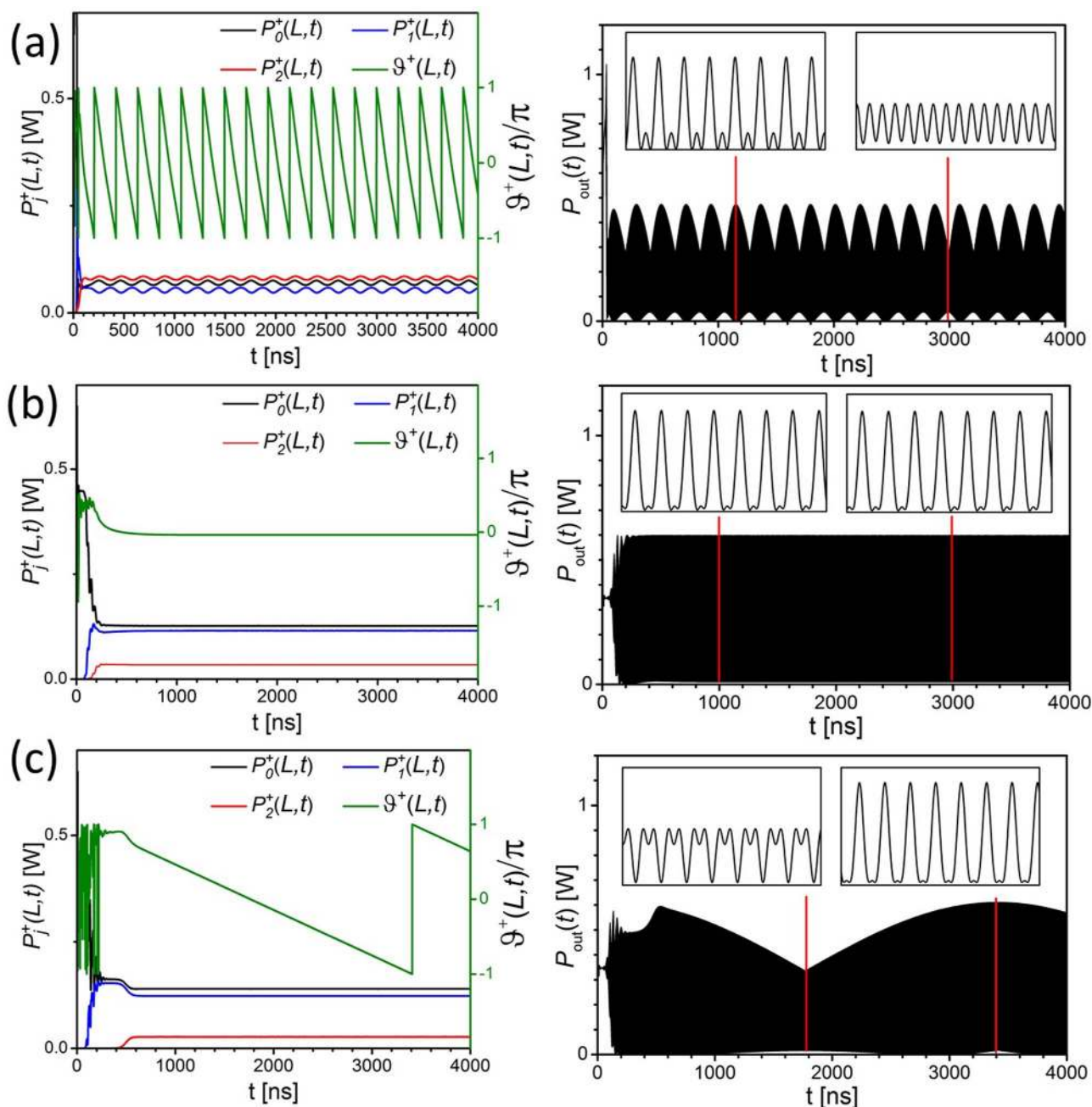


Figure 5 | Simulation Results with and without FWM interaction. Left: Computed temporal evolution of the powers of pump, first and second-order Stokes wave $P_0^+(L,t), P_1^+(L,t), P_2^+(L,t)$, and the phase parameter $\vartheta^+(L,t)$ at the end of the fibre for input power $P_{in} = 0.7$ W. Right: Total output power $P_{out}(t)$. (a) FWM included in the simulation, $\Delta\varphi_0 = 1.2\pi$. (b) FWM included in the simulation, $\Delta\varphi_0 = 0.548\pi$. (c) FWM not included in the simulation, $\Delta\varphi_0 = 0.548\pi$.

$\vartheta^\pm(z,t)$. From the steady state equations it follows that $\vartheta^\pm(z,t)$ must be time-independent, leading to the condition of phase-locking between the three waves. Furthermore, FWM couples the steady state powers to the phases and also the phases to each other via terms containing the phase parameters $\vartheta^\pm(z,t)$. In the absence of FWM the steady state powers $P_j^\pm(z,t)$ are independent of the phases as in a simple Brillouin laser configuration¹⁹. Thus, FWM is crucial to establishing a phase-locked output in the steady state.

In order to generalize these simulation results for a larger parameter space, we performed a two dimensional parameter scan. We chose to scan the input power P_{in} and the parameter $\Delta\varphi_0$ since these parameters are controllable in the experiment for a given fibre sam-

ple by tuning the pump frequency and power. The input power P_{in} was scanned in the interval from 0.4 W to 0.8 W in steps of 0.025 W and the phase shift $\Delta\varphi_0$ from 0 to 2π in steps of 0.05π . For each set of parameters the coupled mode equations were integrated and an analysis (see Methods section for more details) was performed to determine whether the powers $P_j^\pm(z,t)$ and the parameter $\vartheta^+(L,t)$ reach a steady state.

The result of this parameter scan is shown in Fig. 6. The black area corresponds to the case where the phase parameter $\vartheta^+(L,t)$ and the powers $P_j^+(L)$ reach a steady state corresponding to phase-locking and result in a stable interference signal at the output of the fibre. These results qualitatively correspond to the result shown in

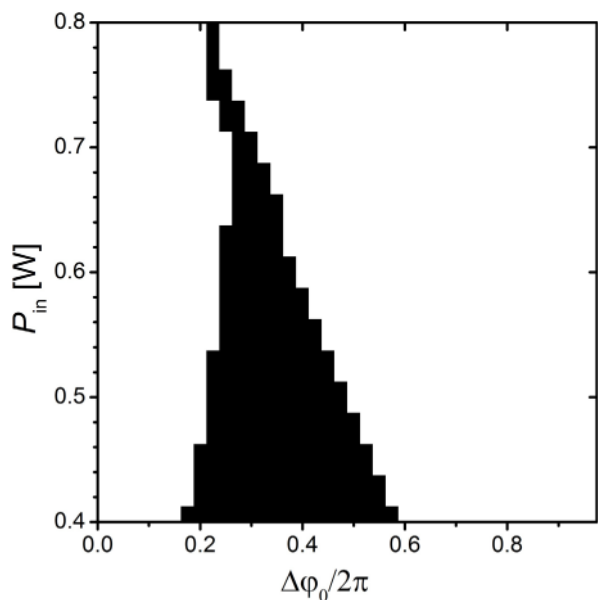


Figure 6 | Domains of phase-locking for different input powers P_{in} and phase shifts $\Delta\phi_0$. Black: Phase-locking ($\partial\vartheta^+(L,t)/\partial t = 0$). White: Drifting phase parameter ($\partial\vartheta^+(L,t)/\partial t \neq 0$).

Fig. 5(b). For the white area in Fig. 6, the parameter $\vartheta^+(L,t)$ does not reach a stable state and no stable interference signals $P_{out}^+(L,t)$ are obtained (similar to the result shown in Fig. 5(a)).

The same parameter scan was also performed for using the coupled mode equations without the FWM terms. We observed that without FWM there is no regime where the parameter $\vartheta^+(L,t)$ reaches a steady state.

Discussion

In this paper, we demonstrated phase-locking of BFCs generated by quasi-CW pumping of a short, low finesse Fabry-Perot resonator (Fig. 2(b)). By repeating the experiment with the same initial conditions we have shown that a mechanism exists that phase-locks the BFC with a particular phase-relationship leading to the generation of stable trains of pulses (Fig. 4). Numerical simulations that included FWM showed a strong qualitative agreement with the experimental results and revealed that FWM is essential for phase-locking and the generation of stable pulse trains. Discrepancies between experimental and simulation results are attributed to uncertainties of experimental parameters and to the neglect of power transfer to higher order (>2) Stokes waves and anti-Stokes waves in the numerical model.

In the experiment, quasi-CW light has been used in order to minimize thermal effects and to achieve high peak powers that are

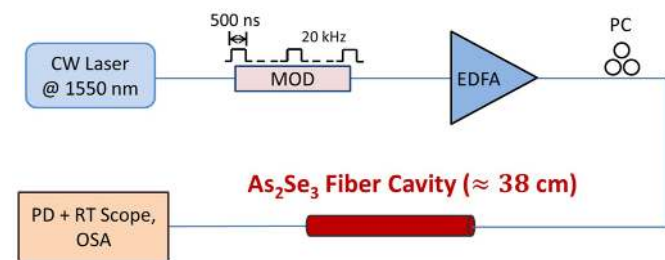


Figure 7 | Schematic of the experimental Setup. MOD: Optical intensity modulator. EDFA: Erbium-doped fibre amplifier. PC: Polarization controller. PD: Photodiode. RT-Scope: Real-time oscilloscope. OSA: Optical spectrum analyser.

necessary in the current configuration. In the future, we will investigate performing the experiment with CW light and explore different configurations that will reduce the necessary peak power. CW generation of the BFC will also allow us to further assess the possibilities of applications and to perform a deeper analysis of the comb stability^{15,35}.

In developing the model we assumed negligible dispersion. This assumption is justified since the cavity length $L \approx 38$ cm is 4 orders of magnitude shorter than the coherence length of the degenerate FWM process³³ $L_{coh} = (2\pi)^2 c / (\lambda^2 \Omega_B^2 D) \approx 4$ km that is calculated using the material dispersion⁴² D of As_2Se_3 .

The frequency detunings of the pump and Stokes waves with respect to the cavity resonances (described by the parameter $\Delta\phi_0$) are sensitive to temperature drift of the resonator leading to a varying output of the resonator on a time scale of a few seconds. Besides active stabilization⁴⁷, reducing the cavity length and therefore increasing the FSR of the cavity could be used to improve stability. Recently, SBS has been demonstrated on photonic chips made of chalcogenide glass exploiting large SBS gain as well as strong mode confinement^{48–50}. Quasi-CW generation of several orders of Stokes waves has been demonstrated on-chip in a low finesse Fabry-Perot cavity of only a few cm length¹⁸. On-chip generation of phase-locked pulse trains via SBS and FWM promises a much higher degree of stability as well as more compact devices and will also be subject of future investigations.

Methods

A schematic of the experimental setup used is shown in Fig. 7. In order to perform the experiment in a quasi-CW regime, the output of a continuous wave laser operating at 1550 nm with a linewidth of 500 kHz was carved into 500 ns square pulses at 20 kHz repetition rate using an optical intensity modulator with extinction ratio of ~ 27 dB. This increased the linewidth of the pump to about 1.8 MHz. The modulator was followed by an erbium doped fibre amplifier (EDFA) to increase the peak intensity of the pulses. Modulating the CW light allowed us to perform the experiment with high peak powers (~ 1 W) while keeping the coupled average power low (~ 10 mW). A polarisation controller was placed after the modulator to align the polarisation of the pump light with a polarisation mode of the chalcogenide fibre resonator. This was achieved by setting the pump power just above the threshold for the generation of the first-order Stokes wave and then adjusting the polarisation such that the power of the first-order Stokes wave is maximised. We used a 38.29 cm long As_2Se_3 step-index fibre (CorActive Inc.) with core and cladding diameters of ~ 5.25 μm and ~ 170 μm , respectively. The numerical aperture of the fibre was $\text{NA} = 0.17$. Light was coupled into and out of the As_2Se_3 fibre by butt-coupling high numerical aperture silica fibres. An optical spectrum analyser (resolution ~ 10 pm) allowed spectral characterization of the output and a photodiode (bandwidth ~ 50 GHz) connected to a real-time oscilloscope (80 GSa/s, bandwidth 33 GHz) enabled real-time analysis of the transmitted signal. The real-time oscilloscope also allowed the recording of 110 consecutive pulse traces. In Fig. 4(a) and 4(b) every tenth trace of such a measurement is plotted.

Details about the coupled mode equations used for the numerical study can be found in the Supplementary Information. For the numerical integration of the time dependent couple mode equations we transformed the variables into frames moving with forward and backward propagating optical fields, respectively^{28,51}, and used the integration method described by de Sterke *et al.*⁵¹. Steady states of the phase parameter $\vartheta^+(L,t)$ and the powers $P_j^+(L,t)$ were determined by integrating the coupled mode equations for a time interval of 6 μs and calculating the standard deviations $\sigma(\vartheta^+)$ and $\sigma(P_j^+)$ of $\vartheta^+(L,t)$ and $P_j^+(L,t)$, respectively, in the time interval [5 μs , 6 μs]. $\vartheta^+(L,t)$ was considered to have reached a steady state if $\sigma(\vartheta^+) < 10^{-3} \times 4\pi$. The power $P_j^+(L,t)$ were considered to have reached a steady state if $\sigma(P_j^+) < 10^{-2} \times \langle P_j^+ \rangle$, where $\langle P_j^+ \rangle$ are the mean values of $P_j^+(L,t)$ in the interval [5 μs , 6 μs].

1. Ippen, E. P. & Stolen, R. H. Stimulated Brillouin scattering in optical fibers. *Appl. Phys. Lett.* **21**, 539–541 (1972).
2. Kobayakov, A., Sauer, M. & Chowdhury, D. Stimulated Brillouin scattering in optical fibers. *Adv. Opt. Photonics* **2**, 1–59 (2009).
3. Agrawal, G. P. *Nonlinear Fiber Optics*. (2006).
4. Hill, K. O., Kawasaki, B. S. & Johnson, D. C. cw Brillouin laser. *Appl. Phys. Lett.* **28**, 608–609 (1976).
5. Stokes, L. F., Chodorow, M. & Shaw, H. J. All-fiber stimulated Brillouin ring laser with submilliwatt pump threshold. *Opt. Lett.* **7**, 509–511 (1982).



6. Grudinin, I. S., Matsko, A. B. & Maleki, L. Brillouin Lasing with a CaF₂ Whispering Gallery Mode Resonator. *Phys. Rev. Lett.* **102**, 043902 (2009).
7. Galindez-Jamioy, C. a. & López-Higuera, J. M. Brillouin Distributed Fiber Sensors: An Overview and Applications. *J. Sensors* **2012**, 1–17 (2012).
8. Kmetik, V. *et al.* Reliable Stimulated Brillouin Scattering Compression of Nd:YAG Laser Pulses with Liquid Fluorocarbon for Long-Time Operation at 10 Hz. *Appl. Opt.* **37**, 7085–7090 (1998).
9. Ottusch, J. J. & Rockwell, D. A. Stimulated Brillouin scattering phase-conjugation fidelity fluctuations. *Opt. Lett.* **16**, 369–371 (1991).
10. Okawachi, Y. *et al.* Tunable All-Optical Delays via Brillouin Slow Light in an Optical Fiber. *Phys. Rev. Lett.* **94**, 153902 (2005).
11. González-Herráez, M., Song, K.-Y. & Thévenaz, L. Optically controlled slow and fast light in optical fibers using stimulated Brillouin scattering. *Appl. Phys. Lett.* **87**, 081113 (2005).
12. Zadok, A., Eyal, A. & Tur, M. Stimulated Brillouin scattering slow light in optical fibers [Invited]. *Appl. Opt.* **50**, E38–E49 (2011).
13. Zhu, Z., Gauthier, D. J. & Boyd, R. W. Stored light in an optical fiber via stimulated Brillouin scattering. *Science* **318**, 1748–1750 (2007).
14. Bahl, G., Tomes, M., Marquardt, F. & Carmon, T. Observation of spontaneous Brillouin cooling. *Nat. Phys.* **8**, 203–207 (2012).
15. Li, J., Lee, H. & Vahala, K. J. Microwave synthesizer using an on-chip Brillouin oscillator. *Nat. Commun.* **4**, 2097 (2013).
16. Zhang, B., Yan, L., Yang, J., Fazal, I. & Willner, A. E. A Single Slow-Light Element for Independent Delay Control and Synchronization on Multiple Gb/s Data Channels. *IEEE Photonics Technol. Lett.* **19**, 1081–1083 (2007).
17. Santagiustina, M., Chin, S., Primerov, N., Ursini, L. & Thévenaz, L. All-optical signal processing using dynamic Brillouin gratings. *Sci. Rep.* **3**(1594), 1–6 (2013).
18. Pant, R. *et al.* Cavity enhanced stimulated Brillouin scattering in an optical chip for multiorder Stokes generation. *Opt. Lett.* **36**, 3687–3689 (2011).
19. Lecoche, V., Randoux, S., Ségard, B. & Zemmouri, J. Dynamics of stimulated Brillouin scattering with feedback. *Quantum Semiclass.* **8**, 1109–1145 (1996).
20. Hill, K. O., Johnson, D. C. & Kawasaki, B. S. cw generation of multiple Stokes and anti-Stokes Brillouin-shifted frequencies. *Appl. Phys. Lett.* **29**, 185–187 (1976).
21. Lamb, R. A., Damzen, M. J. & Wong, G. K. N. Ultrashort pulse generation by phase locking of multiple stimulated Brillouin scattering. *Opt. Commun.* **82**, 337–341 (1990).
22. Shirazi, M. R., Biglary, M., Harun, S. W., Thambiratnam, K. & Ahmad, H. Bidirectional multiwavelength Brillouin fiber laser generation in a ring cavity. *J. Opt. A Pure Appl. Opt.* **10**, 055101 (2008).
23. Cowle, G. J. & Stepanov, D. Y. Multiple Wavelength Generation With Brillouin/Erbium Fiber Lasers. *IEEE Photonics Technol. Lett.* **8**, 1465–1467 (1996).
24. Tomes, M. & Carmon, T. Photonic Micro-Electromechanical Systems Vibrating at X-band (11-GHz) Rates. *Phys. Rev. Lett.* **102**, 113601 (2009).
25. Korolev, F. A., Vokhnik, O. M. & Odintsov, V. I. Mode Locking and Ultrashort Light Pulses in SMBS in an Optical Resonator. *JETP Lett.* **18**, 32–33 (1973).
26. Lugofoi, V. N. Theory of Mode Locking at Coherent Brillouin Interaction. *IEEE J. Quantum Electron.* **19**, 764–749 (1983).
27. Cundiff, S. T. & Ye, J. Colloquium: Femtosecond optical frequency combs. *Rev. Mod. Phys.* **75**, 325–342 (2003).
28. Ogusu, K. & Sakai, A. Generation and Dynamics of Cascaded Stimulated Brillouin Scattering in a High-Finesse Fiber Fabry–Perot Resonator. *Jpn. J. Appl. Phys.* **41**, 609–616 (2002).
29. Boyd, R. W., Rzyzewski, K. & Narum, P. Noise initiation of stimulated Brillouin scattering. *Phys. Rev. A* **42**, 5514–5521 (1990).
30. Dianov, E. M., Isaev, S. K., Kornienko, L. S., Firsov, V. V. & Yatsenko, Y. P. Locking of stimulated Brillouin scattering components in a laser with a waveguide resonator. *Sov. J. Quantum Electron.* **19**, 1–2 (1989).
31. Loranger, S., Iezzi, V. L. & Kashyap, R. Demonstration of an ultra-high frequency picosecond pulse generator using an SBS frequency comb and self phase-locking. *Opt. Express* **20**, 796–798 (2012).
32. Weiner, A. M. *Ultrafast optics*. (2008).
33. Stolen, R. H. & Bjorkholm, J. E. Parametric Amplification and Frequency Conversion in Optical Fibers. *IEEE J. Quantum Electron.* **18**, 1062–1072 (1982).
34. Ferdous, F. *et al.* Spectral line-by-line pulse shaping of on-chip microresonator frequency combs. *Nat. Photonics* **5**, 770–776 (2011).
35. Herr, T. *et al.* Temporal solitons in optical microresonators. *Nat. Photonics* **8**, 145–152 (2013).
36. Russel, T. H. & Roh, W. B. Threshold of second-order stimulated Brillouin scattering in optical fiber. *J. Opt. Soc. Am. B* **19**, 2341–2345 (2002).
37. Tang, J. *et al.* Tunable multiwavelength generation based on Brillouin-erbium comb fiber laser assisted by multiple four-wave mixing processes. *Opt. Express* **19**, 14682–14689 (2011).
38. Al-Alimi, a. W. *et al.* 150-Channel Four Wave Mixing Based Multiwavelength Brillouin-Erbium Doped Fiber Laser. *IEEE Photonics J.* **5**, 1501010 (2013).
39. Cholan, N. a., Al-Mansoori, M. H., Noor, a. S. M., Ismail, a. & Mahdi, M. a. Flattening effect of four wave mixing on multiwavelength Brillouin-erbium fiber laser. *Appl. Phys. B* **112**, 215–221 (2013).
40. Ogusu, K. Interplay between cascaded stimulated Brillouin scattering and four-wave mixing in a fiber Fabry – Perot resonator. *J. Opt. Soc. Am. B* **20**, 685–694 (2003).
41. Holzwarth, R., Zimmermann, M., Udem, T. & Hänsch, T. W. Optical Clockworks and the Measurement of Laser Frequencies With a Mode-Locked Frequency Comb. *IEEE J. Quantum Electron.* **37**, 1493–1501 (2001).
42. Eggleton, B. J., Luther-Davies, B. & Richardson, K. Chalcogenide photonics. *Nat. Photonics* **5**, 141–148 (2011).
43. Abedin, K. S. Observation of strong stimulated Brillouin scattering in single-mode As₂Se₃ chalcogenide fiber. *Opt. Express* **13**, 10266–10271 (2005).
44. Song, K. Y., Abedin, K. S., Hotate, K., Herráez, M. G. & Thévenaz, L. Highly efficient Brillouin slow and fast light using As₂(Se₃) chalcogenide fiber. *Opt. Express* **14**, 5860–5865 (2006).
45. Slusher, R. E. *et al.* Large Raman gain and nonlinear phase shifts in high-purity As₂Se₃ chalcogenide fibers. *J. Opt. Soc. Am. B* **21**, 1146–1155 (2004).
46. Büttner, T. F. S. *et al.* Multi-wavelength gratings formed via cascaded stimulated Brillouin scattering. *Opt. Express* **20**, 26434–26440 (2012).
47. Geng, J. *et al.* Highly stable low-noise Brillouin fiber laser with ultranarrow spectral linewidth. *IEEE Photonics Technol. Lett.* **18**, 1813–1815 (2006).
48. Pant, R. *et al.* On-chip stimulated Brillouin scattering. *Opt. Express* **19**, 8285–8290 (2011).
49. Kabakova, I. V. *et al.* Narrow linewidth Brillouin laser based on chalcogenide photonic chip. *Opt. Lett.* **38**, 3208–3211 (2013).
50. Eggleton, B. J., Poulton, C. G. & Pant, R. Inducing and harnessing stimulated Brillouin scattering in photonic integrated circuits. *Adv. Opt. Photonics* **5**, 536–587 (2013).
51. De Sterke, C. M., Jackson, K. R. & Kenneth, B. D. Nonlinear coupled-mode equations on a finite interval: a numerical procedure. *J. Opt. Soc. Am. B* **8**, 403–412 (1991).

Acknowledgments

The authors thank Prof. Martijn de Sterke for fruitful discussions. Funding from the Australian Research Council (ARC) through its Laureate Project FL120100029 is gratefully acknowledged. This research was also supported by the ARC Center of Excellence for Ultrahigh Bandwidth Devices for Optical Systems (project number CE110001018). D. Hudson acknowledges support from an ARC Discovery Early Career Research Award (DE130101033).

Author contributions

B.J.E., T.F.S.B., I.V.K. and R.P. conceived the experiment. T.F.S.B. and I.V.K. carried out the experiment. T.F.S.B., I.V.K., A.C.J. and C.G.P. discussed the theory and the simulation method. T.F.S.B. carried out the numerical simulations. T.F.S.B. wrote the manuscript and prepared the figures. B.J.E., I.V.K., A.C.J., C.G.P. and D.D.H. edited the manuscript. B.J.E., D.D.H. and I.V.K. supervised the project. All authors discussed the results and commented on the manuscript.

Additional information

Supplementary information accompanies this paper at <http://www.nature.com/scientificreports>

Competing financial interests: The authors declare no competing financial interests.

How to cite this article: Büttner, T.F.S. *et al.* Phase-locking and Pulse Generation in Multi-Frequency Brillouin Oscillator via Four Wave Mixing. *Sci. Rep.* **4**, 5032; DOI:10.1038/srep05032 (2014).



This work is licensed under a Creative Commons Attribution-NonCommercial-ShareAlike 3.0 Unported License. The images in this article are included in the article's Creative Commons license, unless indicated otherwise in the image credit; if the image is not included under the Creative Commons license, users will need to obtain permission from the license holder in order to reproduce the image. To view a copy of this license, visit <http://creativecommons.org/licenses/by-nc-sa/3.0/>